Journal of Biomedical Optics

SPIEDigitalLibrary.org/jbo

Real-time label-free detection of dividing cells by means of lensfree video-microscopy

Srikanth Vinjimore Kesavan
Fabrice P. Navarro
Mathilde Menneteau
Frederique Mittler
Brigitte David-Watine
Nelly Dubrulle
Spencer L. Shorte
Bernard Chalmond
Jean-Marc Dinten
Cedric P. Allier

SPIE

Real-time label-free detection of dividing cells by means of lensfree video-microscopy

Srikanth Vinjimore Kesavan,[a] Fabrice P. Navarro,[a] Mathilde Menneteau,[a] Frederique Mittler,[a] Brigitte David-Watine,[b] Nelly Dubrulle,[b] Spencer L. Shorte,[b] Bernard Chalmond,[c,d] Jean-Marc Dinten,[a] and Cedric P. Allier[a,*]

[a]Commissariat à l'énergie atomique et aux énergies alternatives (CEA), LETI, MINATEC, 17 rue des martyrs, Grenoble cedex 9, 38054 France
[b]Plateforme d'imagerie dynamique, Imagopole, Institut Pasteur, Paris, 75015 France
[c]University of Cergy-Pontoise, UFR Sciences, Cergy 95011 France
[d]CMLA, École Normale Supérieure de Cachan, 94230 France

Abstract. Quantification of cell proliferation and monitoring its kinetics are essential in fields of research such as developmental biology, oncology, etc. Although several proliferation assays exist, monitoring cell proliferation kinetics remains challenging. We present a novel cell proliferation assay based on real-time monitoring of cell culture inside a standard incubator using a lensfree video-microscope, combined with automated detection of single cell divisions over a population of several thousand cells. Since the method is based on direct visualization of dividing cells, it is label-free, continuous, and not sample destructive. Kinetics of cell proliferation can be monitored from a few hours to several days. We compare our method to a standard assay, the EdU proliferation assay, and as proof of principle, we demonstrate concentration-dependent and time-dependent effect of actinomycin D—a cell proliferation inhibitor. [DOI: 10.1117/1.JBO.19.3.036004]

Keywords: lensfree video-microscopy; label-free cell proliferation assay; real-time cell culture monitoring; cell proliferation kinetics.

Paper 130836R received Nov. 22, 2013; revised manuscript received Jan. 8, 2014; accepted for publication Jan. 23, 2014; published online Mar. 5, 2014.

1 Introduction

Cell division is one of the main events determining cell fate. Cell proliferation rate can reveal important information on perturbation of the cell cycle and is used routinely in a variety of biomedical research areas, including oncology and drug discovery. Current cell proliferation assays quantify proliferation either directly by incorporating a modified nucleotide (BrdU/EdU) to the newly synthesized DNA (at S phase of cell cycle)[1–3] or indirectly by measuring parameters such as total ATP/DNA content,[4–6] metabolic rate,[7,8] substrate impedance changes,[9–12] etc. Most of the direct techniques are static end point assays. Hence, they do not allow the measurement of cell proliferation kinetics—a critical parameter to test the time-dependent effect of various drugs/agents on cell proliferation. Other limitations include dependency on markers, being cumbersome, and being sample destructive. Indirect techniques are unsatisfactory, as strong assumptions are needed to correlate surrogate measurements with single cell division. The simplest way to measure cell proliferation rate would be to count individual cell divisions in a cell population as and when it occurs. Only very few methods have been proposed so far to quantify/analyze cell division on the basis of time-lapse imaging.[13–17] However, the limitations include limited field of view (FOV), high cost and decreased feasibility of the approach, phototoxicity, and photobleaching.

Here, we propose a new method, coined "lensfree video proliferation assay," based on continuous and high-throughput recording of cells in culture using lensfree video-microscopy (see Sec. 2). It features the automated detection of dividing cells among a population of thousands of cells at a glance, which overcomes the drawbacks of existing methods. Unlike the currently used proliferation assays, cell division is directly detected without the need for surrogate measurements, exogenous contrast agents, or fluorescent dyes. Further, it is practical and highly amenable to facilitate high throughput inasmuch as it (1) does not require cell harvesting and (2) provides continuous direct live imaging data to follow cell proliferation kinetics as they happen in thousands of cells, yielding robust statistics outright.

To validate our methodology, we compare the results obtained from lensfree video proliferation assay and classical EdU proliferation assay. We further confirm the approach by testing its capacity to follow the changes in proliferation kinetics induced by treating the cells with a cell proliferation inhibitor.

2 Materials and Methods

2.1 *Lensfree Video-Microscopy*

Lensfree video-microscopy mentioned here implements in-line holographic imaging technique, which is explored extensively of late.[18–23] It consists of a 12-bit APTINA MT9P031 CMOS RGB imaging sensor with a pixel pitch of 2.2 μm, measuring 5.7×4.3 mm, and light-emitting diode (LED) (dominating wavelength 525 nm) with a pinhole of 150 μm. In a typical experiment, the lensfree video-microscope is placed inside the incubator and the petri dish containing the cells is placed on lensfree video-microscope. Illumination is provided by the LED along with the pinhole from a distance of ~5 cm. The light scattered by the sample and the light passing directly from the source to the imaging sensor interfere to form

*Address all correspondence to: Cédric P Allier, E-mail: cedric.allier@cea.fr

0091-3286/2014/$25.00 © 2014 SPIE

a holographic pattern, which is recorded by the sensor. A USB cord connecting the laptop and the system passes through the provision at the rear of the incubator (Fig. 1).

2.2 *Cell Culture*

Murine NIH3T3 fibroblasts were obtained from the American Type Culture Collection and were grown in Dulbecco's modified Eagle's medium (DMEM) supplemented with 10% newborn calf serum (PAN Biotech, Aidenbach, Germany) and 1% antibiotics (penicillin and streptomycin) (Gibco, Life Technologies, Saint-Aubin, France). Primary cultures of human fibroblasts prepared from skin biopsies performed on healthy donors (male, 30 to 39 years) were established in DMEM-Glutamax (Invitrogen, Life Technologies, Saint-Aubin, France) supplemented with 20% fetal calf serum (FCS) and used at passage 2. Nemo$^{-/-}$ (seeding density: 30,000 cells) cells are SV40 immortalized human fetal female fibroblasts with a mutant Nemo gene (a gift from Dr. A. Smahi). Vero cells (a gift from F. Barre-Sinoussi's lab) (seeding density: 26,000 cells) are kidney cells from *Cercopithecus aethiops*. BJ newborn foreskin fibroblasts are from the American Type Culture Collection. Cells (Nemo, Vero, 343, BJ) were grown in DMEM Glutamax plus 10% FCS.

2.3 *Comparison of Lensfree Video Proliferation Assay with Standard EdU Proliferation Assay*

A standard 35-mm petri dish was filled with 2.5 ml of culture media at a cell density of 2.5×10^4 cells/ml. For cell incubation with EdU, cells were seeded on day 1 in DMEM supplemented culture media with 10% FCS. Cells were treated on day 2 with 10 μM EdU (Click iT® EdU Invitrogen) followed by 2.5-h incubation. The petri dish was imaged with lensfree video-microscope during EdU incubation period. Following the incubation period, EdU was removed through three washes in phosphate-buffered saline (PBS) and cells were transferred in tubes after trypsin (Gibco) treatment. According to manufacturer's recommendation, cells were fixed in 1 ml 1% formaldehyde (Sigma-Aldricha, L'Isle d'Abeau, Chesnes, Saint-Quentin Fallavier, France). After 15 min, cells were washed once in PBS/1% bovine serum albumin (BSA). Then, cells were treated for 30 min with 1× saponin solution for membrane permeabilization. After washing once in PBS containing 1% BSA, cells were centrifuged at 500 g for 5 min and supernatant was eliminated. Cells were incubated for 30 min at room temperature in the dark in presence of the click cocktail reaction buffer containing the fluorescent dye (Invitrogen). After washing and centrifugation at 500 g for 5 min, cells were harvested and stored at 4°C until fluorescence activated cell sorting (FACS) analysis.

2.4 *Inhibiting Cell Proliferation Using Actinomycin D*

A standard 35-mm petri dish was filled with 2.5 ml of culture media at a cell density of 2.5×10^4 cells/ml. Cells were seeded in three petri dishes on day 1. On day 2, actinomycin D (ActD) was added at concentrations of 0 μg/ml (untreated control), 5 μg/ml, and 10 μg/ml. The petri dishes were imaged simultaneously by three lensfree video-microscopes immediately following the administration of the drug for a period of 6.5 h. Similarly, three petri dishes were prepared in parallel adhering to the same protocol for EdU proliferation assay. EdU was added for the final 2.5 h without changing the concentration of ActD.

2.5 *Monitoring Cell Proliferation Kinetics*

A standard 35-mm petri dish was filled with 2.5 ml of culture media at a cell density of 2.5×10^4 cells/ml. Cells were seeded on day 1. On day 2, cells were imaged using lensfree video-microscope from ~4.5 h before the addition of ActD (at 2.5, 1, and 0.5 μg/ml) until ~4.5 h following the addition of the drug.

2.6 *FACS Analysis*

EdU-incorporated cells were analyzed using a BD LSR II two-laser flow cytometer (BD Biosciences, San Jose, California). The red laser (633 nm) is used for the detection of Alexa Fluor® 647. Sample measurements were performed with DIVA® software (BD Biosciences). Cell debris and aggregates were excluded from the analysis using an appropriate threshold (~30,000).

2.7 *Computational Methods*

For pattern recognition, a typical holographic pattern obtained from a dividing metaphase cell was chosen to act as a template. Using normalized cross-correlation function available in MATLAB® with a constant threshold, the template was matched with the full FOV image of 24 mm^2, and the cells exhibiting similar holographic patterns were recognized and counted.

Fig. 1 Schematic diagram (a) and photograph of lensfree video-microscope (b) that is used to obtain time-lapse images inside the incubator. Red arrows indicate lensfree video-microscopes placed inside a standard incubator (c).

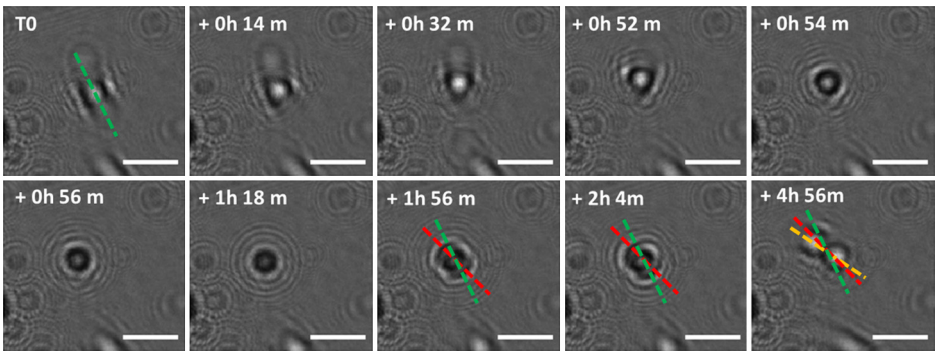

Fig. 2 Temporal images of interest from real-time monitoring of a BJ cell (Video 1) showing the change in cell shape and cell adhesion taking place during cell division. Cell rounding can be observed in images obtained at T0 + 0 h 52 min and T0 + 0 h 54 min. Reduced cell substrate adhesion leading to signature holographic pattern of a dividing cell can be seen in images T0 + 0 h 56 min and T0 + 1 h 18 min. Cytokinesis and separation of daughter cells can be seen from T0 + 1 h 56 min until T0 + 4 h 56 min. Diagonal (dotted) green line indicates the longest axis of the cell prior to cell division. Red line denotes the cell division axis during cytokinesis. Yellow line denotes the axis of separation of daughter cells. The cell in this case has divided along the longest axis prior to cell division. Scale bar: 100 μm.

To estimate the total number of cells present in an image (dividing and nondividing), the obtained image was converted to its binary form. Using constant appropriate thresholding based on gray-level, area, major, and minor axis lengths, holographic patterns corresponding to cells were identified and counted.

Percentage of dividing cells is the ratio of total number of dividing cells to average total number of cells calculated from images obtained over a period of time (typically 2.5 h). A period of 2.5 h was chosen in order to be in concurrence with the EdU incubation period of 2.5 h.

In cases of highly confluent cultures, the typical holographic signature corresponding to metaphase might be masked and left undetected. In these cases, cell retraction was used as a way to detect dividing cells. Retracting cells exhibit a pattern where the center of the holographic pattern is bright, while the edges are dark (Fig. 2, images at T0 + 0 h 52 min and T0 + 0 h 54 min). By detecting these alternating bright and dark intensity regions in an image, retracting cells were identified (Video 1).

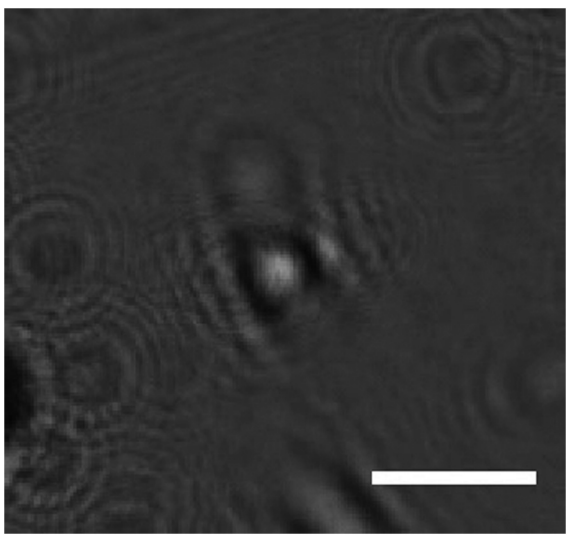

Video 1 Changes in cell shape and cell adhesion during cell division from the perspective of lensfree video-microscope. Frames were obtained every 2 min for ~5.5 h. Cell rounding and reduced cell-substrate adhesion during cell division gives a typical holographic pattern, which is considered as the signature for mitotic cells. Cell retraction, cell rounding, reduction in cell-substrate adhesion, cytokinesis, and separation of daughter cells of a BJ cell is observed. Scale bar: 100 μm. (mov, 419 KB) [URL: http://dx.doi.org/10.1117/1.JBO.19.3.036004.1].

3 Results

3.1 *Real-Time Monitoring of Cell Culture and Automated Detection of Dividing Cells*

Lensfree video-microscope works using the principle of in-line holography (Sec. 2). The absence of magnification lenses renders large FOV of 24 mm^2 covering several thousand cells. Lensfree video-microscope is placed inside a standard incubator (as shown in Fig. 1) to monitor cell culture in real time.

The automated detection of dividing cells using lensfree video-microscopy is based on the changes in shape and adhesion that mitotic cells undergo. Before dividing into two

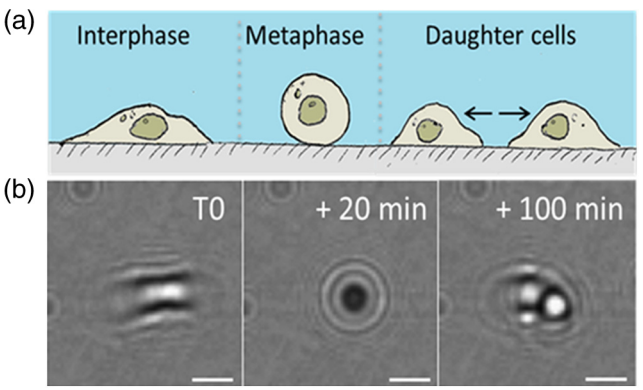

Fig. 3 (a) Schematic drawing showing the change in cell shape during cell division typifying a process called mitotic cell rounding. (b) Cell rounding and reduction in cell-substrate adhesion preceding the separation of daughter cells is clearly observed in the hologram obtained from the NIH 3T3 cell at T = T0 + 20 min. The two daughter cells are seen at T = T0 + 100 min. Scale bar: 50 μm.

daughter cells, almost all mammalian cells undergo dramatic shape transformation from being flat during interphase to being round during M phase, typifying a process termed "mitotic cell rounding." This is usually accompanied by a reduction in cell-substrate adhesion. A schematic drawing illustrating changes in cell shape and substrate adhesion during division is presented in Fig. 3(a). Upon entering mitosis, the complex actin network is completely deconstructed and re-formed.[24] Hence, at metaphase, during mitosis, the cells adopt a round shape and a decreased adhesion to the substrate.[25–29] This helps in efficient and stable bipolar spindle formation and is, thus, vital to ensure a proper cell division.[30] Almost all proliferating animal cells undergo these changes before cytokinesis. While extensive research has aimed to understand the underlying mechanism of the driving force(s) leading to cell rounding,[31–36] these changes have not been exploited as a signature of mitotic cells. By contrast, lensfree video proliferation assay exploits the change in cell shape and cell adhesion as a natural marker to detect dividing cells. Jin et al. also mentioned the changes in the holographic pattern corresponding to the changes in cell morphology during cell division,[22] but it was not exhaustively studied.

It is to be noted that the holographic pattern obtained from a floating cell is different from the holographic pattern obtained from an adherent cell. When the cell is not adhered to the substrate, the holographic pattern obtained from the cell is similar to an airy pattern. The zero-order gray-level value is lower and interference rings are observed. In contrast, for an adherent cell, the zero-order gray level reaches larger values and the holographic pattern obtained is different. These changes can, hence, be observed during cell division as there is reduction in cell-substrate adhesion. To exemplify the approach, a montage of the recorded holographic pattern of a dividing NIH3T3 cell observed using the lensfree video-microscope is shown in Fig. 3(b). At $T = T0$, the cell is elongated and adhered to the substrate with larger zero-order gray-level value. There is a sharp change in the holographic pattern obtained from the cell at $T = T0 + 20$ min. The zero-order gray level reaches a lower value denoting reduction in cell-substrate adhesion. The daughter cells are observed at $T = T0 + 100$ min. All the cells that experience rounding and reduction in cell-substrate adhesion during division exhibit a similar holographic pattern [as in Fig. 3(b), $T = T0 + 20$ min]. Thereafter, cells that are in the process of division are identified among several thousand neighboring cells by pattern recognition (FOV of the image 24 mm^2) [Fig. 4(a)]. In some cases, the pattern corresponding to cell division may appear in subsequent temporal images. These repetitive events, though not counted, are marked by yellow squares [Figs. 4(a), 4(b), and 4(c)]. We have verified the accuracy of the automated detection of patterns by manually detecting the patterns and by following it in the subsequent temporal images to ensure the occurrence of cell division. Since true negatives cannot be determined in this case, we calculated the F1 measure (harmonic mean of precision and recall with equal weightage) based on true positives, false positives, and false negatives. True positives constitute accurate automated detection of patterns from cells that further divide in the subsequent temporal images. False positives constitute erroneous detection of patterns, which either were not from cells or were from cells that did not divide in the subsequent temporal images. False negatives are the cell divisions that were missed. The F1 measure is close to 0.87 on a scale of 0 to 1, with 1 being the best score. The measurement was based on seven random sequences of nine images that are temporally separated by 20 min, of dimension 1900×1425 μm, from different independent experiments (Table 1).

3.2 *Comparison of the Lensfree Video Proliferation Assay with Standard EdU Proliferation Assay*

In order to validate the method, it was directly compared to the standard EdU proliferation assay. Cells were imaged using the lensfree video-microscope inside an incubator during the EdU incubation period of 2.5 h. The acquired images were subjected

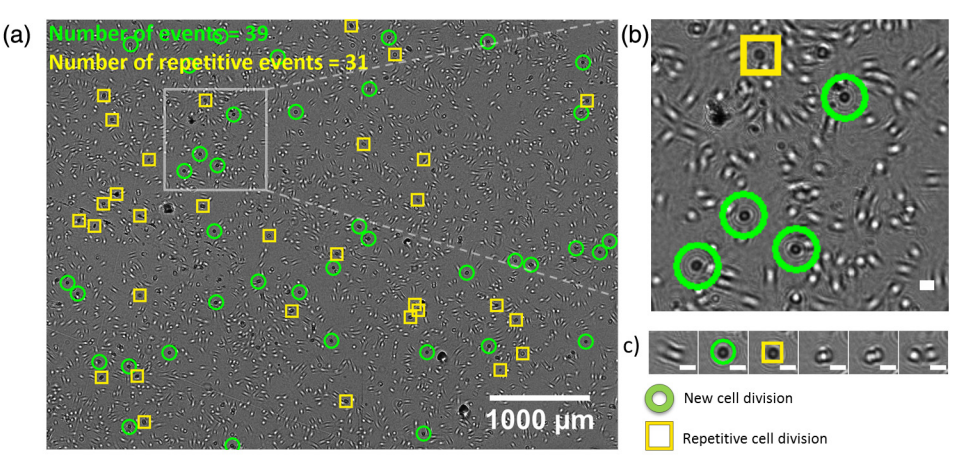

Fig. 4 (a) Number of cells exhibiting the pattern corresponding to cell division is detected using pattern recognition in a full field of view image of 24 mm^2, spanning across several thousand cells. New cell divisions are encircled in green, while repetitive cell divisions (cells that were round from the previous image) are marked in yellow squares. (b) Magnified region of interest showing cells that are encircled in green and marked in yellow squares among adherent (bright holographic pattern) neighboring cells. Scale bar: 50 μm. (c) Time-lapse images showing a cell exhibiting the pattern corresponding to cell division in subsequent temporal images (temporally separated by 20 min). Initially, the cell is encircled in green and later it is marked in yellow square. Scale bar: 50 μm.

to pattern recognition. A total of nine images were acquired per experiment. The number of cells undergoing division was calculated for each image and was summed. In order to compare the results obtained with the two assays, the total number of dividing cells calculated with the lensfree video proliferation assay was divided by the average total number of cells that were present in the images to yield the percentage of dividing cells. Automated detection of the total number of cells (in dividing and nondividing cells) was based on binary conversion of the image and an appropriate threshold to remove noise. The number of cells from random images was manually calculated to verify the accuracy of automated detection (Table 1). Six independent experiments were performed. It was observed [Fig. 5(a)] that the proliferation rate (percentage of dividing cells) obtained using our method is $18 \pm 5\%$ (s.d. $n = 6$ experiments), whereas the proliferation rate obtained using EdU proliferation assay is $33.8 \pm 6\%$ (for the EdU incubation period of 2.5 h). The difference in the results could be due to false positives from EdU proliferation assay or false negatives from lensfree video proliferation assay (or both). EdU proliferation assay detects the cells that are in the initial stage of cell division (S phase). False positives may occur in EdU proliferation assay if a cell that is marked during the S phase is stopped from dividing at the G2-M checkpoint [Fig. 5(b)] due to improper replication of DNA. Indeed the cells are allowed to pass through the checkpoints only after they have repaired DNA damages.[37–39] Lensfree video proliferation assay detects the cells that are in the final process of cell division (M phase) and is unbiased by the G2-M checkpoint. However, false negatives may occur if holographic signature corresponding to mitosis is not well detected. Also, the temporal resolution of the experiments performed was 20 min; this may have also limited the detection efficiency causing false negatives. Nevertheless, the standard deviation of the proliferation rate measurement over $N = 6$ experiments is 5%, showing the consistency of the method comparable to that of EdU proliferation assay. Further, the impact of a cell proliferation inhibitor is clearly depicted in the results obtained by the method (Sec. 3.3). Though we cannot claim that the method is quantitative at this stage, it is qualitative and can monitor the differences in cell proliferation, which is essential in various studies, especially drug/siRNA screening.

3.3 *Inhibiting Cell Proliferation Using Actinomycin D*

The rate of cell proliferation may be altered by various stimulating or inhibiting conditions or agents. We further assessed our methods by measuring the influence of ActD, which is well known for inhibiting cell proliferation.[40,41] ActD was added to culture plates at predetermined concentrations of 0 μg/ml (control), 5 μg/ml, and 10 μg/ml. Following the administration of the drug, the culture plates were imaged in parallel using three lensfree video-microscopes (as shown in Fig. 1) for 6.5 h. Images were acquired every 20 min, and the obtained images were subjected to pattern recognition to calculate the number of dividing cells. It is noteworthy that manipulation of the culture plates during the addition of the drug triggered the detachment of a few cells that also gave rise to a holographic pattern similar to the one corresponding to cell division. In order to avoid the interference of these floating cells in the calculation, the initial three images following the addition of the drug were not considered for measurement.

The number of dividing cells was calculated for a total of 324 images obtained from six independent experiments, with 108 images per condition (control, 5 μg/ml, and 10 μg/ml). As shown in the graphs (Fig. 6), the number of dividing cells was, on an average, between 30 and 40 per image for untreated cells, and a total of 625 ± 66 (s.d. $n = 6$ experiments) cells divided during the experiment time frame. On the contrary, the number of dividing cells was reduced to <5 per image for cell cultures treated with 5 and 10 μg/ml of ActD, within the initial 3 h following the addition of the drug. Only 48 ± 17 and 34 ± 15 (s.d. $n = 6$ experiments) cells divided in cell populations treated with the drug at concentrations of 5 and 10 μg/ml, respectively. Thus, the impact of the presence of the drug on the number of dividing cells could be demonstrated but with little or no variation of the effect at different concentrations of the drug.

We verified the results obtained by lensfree video proliferation assay using EdU proliferation assay. The average percentage of dividing cells for the control was $45 \pm 4\%$ (s.d. $n = 6$ experiments) during the 2.5 h EdU incorporation time. On the complete contrary, average percentage population of dividing cells in the presence of the ActD (5 and 10 μg/ml) was close to zero (Table 2). Hence, similar to the results obtained by lensfree video proliferation assay, no difference could be observed between the two drug concentrations.

3.4 *Monitoring Cell Proliferation Kinetics*

The most expected contribution from any cell proliferation assay, and the least met with, is to give an accurate description of the kinetics of cell proliferation and its variations. By monitoring cell cultures before and after the addition of ActD, we are able to show how lensfree video proliferation assay meets this critical requirement. To give an accurate description of the kinetics of cell proliferation and its variations, influenced by different concentrations of ActD, cell cultures were monitored before (4.5 h) and immediately after the addition of ActD (for 4.5 h) at smaller concentrations (compared to previously used 5 and 10 μg/ml) of 2.5, 1, and 0.5 μg/ml (Fig. 7). In the case of 2.5 μg/ml, the average total number of cell divisions (for a period of 4.5 h) before and after the addition of the drug were 433 ± 112 and 63 ± 7 (s.d. $n = 4$), respectively. The average total number of dividing cells was reduced by ~80%. As expected, when the concentration was further reduced to 1 and 0.5 μg/ml, the effect was less pronounced. The average total number of cell divisions before the addition for 1.0 and 0.5 μg/ml were 310 ± 35 and 327 ± 18 (s.d. $n = 4$), respectively. After the addition of the drug, the average total number of dividing cells was reduced by ~50% in both the cases (128 ± 34 and 131 ± 14 for 1 and 0.5 μg/ml, respectively). These results demonstrate a rapid effect of ActD on cell proliferation at 2.5 μg/ml, compared to a more gradual effect at 1 and 0.5 μg/ml.

3.5 *Application to Other Cell Types Including Primary Cells*

To test the versatility of the lensfree video proliferation assay, we followed the proliferation kinetics of other cell types: primary human fibroblasts (343), immortalized human fetal fibroblasts (Nemo$^{-/-}$), and Vero cells. Cells were allowed to adhere to the substrate for 4 h following cell plating. We calculated the

Table 1 Validation of automated pattern recognition of dividing cells and automated cell count.

Validation of pattern recognition of dividing cells							
No. of dividing cells (Manual count)	Automated count	True Positives (TP)	False Positives (FP)	False Negatives (FN)	Precision (P) [TP/(TP + FP)]	Recall (R) [TP/(TP + FN)]	Fl Measure [2PR/{P + R)]
176	173	156	17	20	0,90	0,84	0,87
Validation of automated cell count: Number of cells present in an image (dividing + nondividing)							
Total no. of cells (Manual count)	Automated count	True Positives (TP)	False Positives (FP)	False Negatives (FN)	Precision (P) [TP/(TP + FP)]	Recall (R) [TP/(TP + FN)]	Fl Measure [2PR/(P + R)]
1177	1152	1118	34	59	0,97	0,94	0,95

Note: For the validation of pattern recognition of dividing cells, seven random sequences of nine images (temporal resolution 20 min) of dimension 1900×1425 μm from different independent experiments were considered. Automated detection was compared to manual detection.
For the validation of cell count, 10 random images of dimension 1196×1050 μm from random independent experiments were considered. Automated detection was compared to manual detection.
Precision or positive predictive value is defined as $TP/(TP + FP)$, while recall or sensitivity is defined as $TP/(TP + FN)$, where TP, FP, and FN are true positives, false positives, and false negatives, respectively. F1 measure is the harmonic mean of precision and recall with equal weightage.

percentage of cell division or proliferation rate. Percentage of cell proliferation is the ratio of number of dividing cells to average total number of cells calculated from images acquired over a period of 2.5 h. We followed the kinetics for over 12 h. A moving average of the percentage of dividing cells (with a period of ~2.5 h) was plotted. To be in accordance with our previous calculation of the percentage of dividing cells for NIH3T3 cells (in Sec. 3.2), 2.5 h was chosen as a period for moving graph. It could be inferred (Fig. 8) that the percentage of dividing cells for immortalized cell line Nemo$^{-/-}$ is higher compared to Vero and primary human fibroblasts (343).

4 Discussion

Lensfree video proliferation assay serves as a simple and a direct method to count dividing cells in a cell population. Since the system is placed inside an incubator for time-lapse imaging, there is no need for specialized chambers, as required by standard video-microscopy, to maintain ambient conditions for the cells. Cell populations can be monitored from a few hours to several days for the purpose of defining cell proliferation kinetics on the basis of which factors that would induce or inhibit cell proliferation can be tested. Here we demonstrated the effect of different concentrations of ActD, a well-known cell proliferation inhibitor, on cell populations for a period of 5 to 7 h. From the results, we could observe that even though the concentration of ActD administered differed considerably, cell populations reacted the same by suffering a large inhibition of cell division within the first 3 h following the addition of ActD; the difference in the concentration of the drug (10, 5, and 2.5 μg/ml) only had a negligible impact. Conclusions could be drawn either based on the number of dividing cells per image or based on the percentage of dividing cells calculated over a period of time. In cases where cell seeding density is known and is the same across the samples to be tested, the former could be used, while otherwise the latter could be employed.

The acquired raw image can be reconstructed to obtain minute details.[18] However, since the changes in cell shape and cell-substrate adhesion are well exhibited in the raw image, holographic reconstruction is not necessary for the detection of dividing cells. Nevertheless, it is a promising tool to further analyze single cell divisions with greater detail, which would be a future perspective.

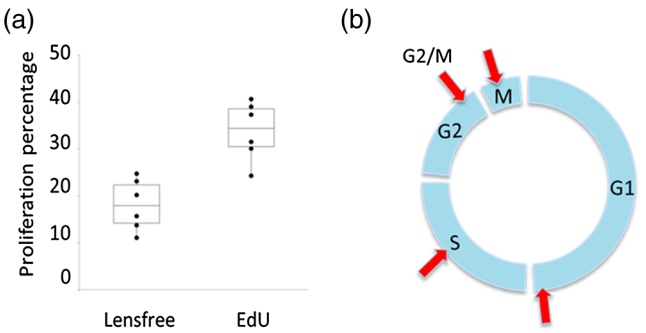

Fig. 5 (a) Percentage proliferation rate measured by lensfree video proliferation assay and EdU proliferation assay. Data points obtained from six independent experiments are shown. The horizontal line in the plot marks the median. Error bar s.d., six independent experiments. (b) Cell cycle showing different checkpoints at various stages (marked by red arrow). EdU proliferation assay detects cells that are in the initial stage of division (S phase), whereas lensfree video proliferation assay detects cells that are in the final stage of cell division (M phase).

4.1 *Applicability of the Approach to Various Other Cell Types*

We have tested the approach with various other cell types, such as Vero, U87, RPE1, RWPE1, primary human fibroblasts, mesenchymal stem cells, PC3, HUVEC, and MCF10A cells in both two-dimensional (2-D) and three-dimensional (3-D) cell culture conditions (Fig. 9) and shown that the method is applicable to numerous cell types in 2-D cell culture. Since the cells in 3-D cell culture do not show enhanced substrate adherence as in 2-D, the change in the holographic pattern is less pronounced. The approach is not applicable to floating cells, such as hematopoietic cells, but it is to be noted that majority of the cell types are adherent to the substrate in nature.

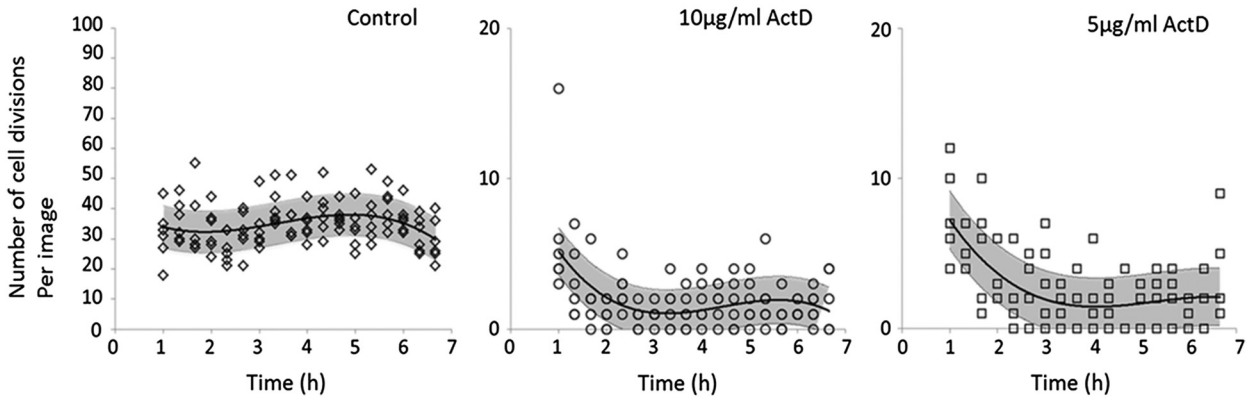

Fig. 6 Number of dividing cells calculated for three different conditions from six independent experiments is plotted. Trendline of polynomial order 3 of mean is shown. The number of cell divisions in an image is between 30 and 40 in the case of control, whereas in the case of 10 μg/ml actinomycin D (ActD) and 5 μg/ml ActD, the number of cell divisions per image is reduced to <5 denoting a strong effect of the drug.

4.2 *Implementing the Performance of the System*

In the first version of the lensfree video-microscope, images could only be acquired at 20-min intervals. Because of overheating of the sensor, the microscope had to be switched off in between acquisitions to keep the cells from the exposure to heating of the sensor. During image acquisitions (which takes only a few seconds), a small fan installed was switched on to reduce the heating. In the more recent version of the lensfree video-microscope, a Peltier device was added to maintain ambient temperature (37°C) at the sensor surface, thus permitting to perform image acquisitions at will. As with the lensfree video-microscope, not any label or fluorescent reporter is needed, and because the system does not use lasers, there are no special concerns about phototoxicity for the cells or photobleaching of reporters. Using this device, we performed 1-min-interval image acquisitions. This permitted us to image various stages of cell division, such as cell retraction, cell rounding, reduction in cell-substrate adhesion, cytokinesis, and separation of daughter cells of a BJ cell (Fig. 2, Video 1). Hence apart from detecting dividing cells, analysis on cell division could be performed through label-free tracking of thousands of single cells from cell retraction until separation of daughter cells, providing an entirely new perspective on cell division that includes determination of time taken at each of the above-mentioned steps to investigate any delay in cell division, determination of cell division axis, etc. The cell division axis determines the fate of the daughter cells, and several parameters controlling the cell division axis, such as cell geometry[42] and environment,[43] are being investigated.[44–46] Lensfree video-microscope can be used as a tool to determine the cell division axis in thousands of single cell divisions (Fig. 2). It can be observed that in the particular

Table 2 EdU proliferation assay to verify the influence of actinomycin D (ActD).

	Control			5 μg/ml ActD			10 μg/ml ActD		
Independent Experiments 00	Total number of events	Number of dividing cells	Percentage of dividing cells	Total number of events	Number of dividing cells	Percentage of dividing cells	Total number of events	Number of dividing cells	Percentage of dividing cells
1	10,000	4113	43.3	10,000	18	0.2	10,000	6	0.1
2	10,000	3856	41.3	10,000	3	0.0	10,000	1	0.0
3	10,000	4249	45.0	10,000	14	0.1	10,000	14	0.1
4	10,000	4629	49.1	10.000	1	0.0	10,000	8	0.1
5	10,000	4879	51.7	10,000	13	0.1	10,000	3	0.0
6	10,000	3876	42.2	10,000	4	0.0	10,000	0	0.0

Note: The table was drawn to depict the results obtained from FACS analysis. EdU-incorporated cells were analyzed using a BD LSR II two-laser flow cytometer (BD Biosciences). The red laser (633 nm) is used for the detection of Alexa Fluor® 647. Sample measurements were performed with DIVA® software (BD Biosciences). Cell debris and aggregates were excluded from the analysis using an appropriate threshold (~30,000). Based on the results obtained from six independent experiments, the average percentage of dividing cells for the control (untreated with ActD) was 45 $\pm$ 4% (s.d. $n = 6$ experiments) during the 2.5-h EdU incorporation time. On the complete contrary, average percentage population of dividing cells in the presence of the ActD (5 and 10 μg/ml) was close to zero. Hence, similar to the results obtained by lensfree video proliferation assay, though drastic difference is seen between cells exposed to ActD and those which were not, no difference could be observed in the influence of the drug at two concentrations.

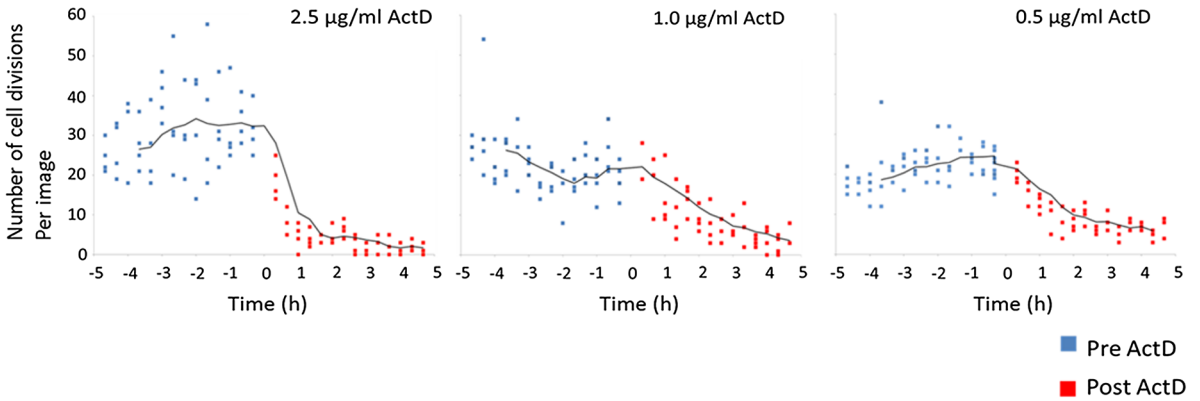

Fig. 7 Cell cultures subjected to different concentrations of ActD were monitored for a period of ~9 h before and after the addition of ActD. Time T = 0 h marks the addition of the drug. Trend line of order 4 of the mean number of cell divisions per image plummets immediately following the addition of the drug in the case of 2.5 μg/ml, whereas a more gradual decrease is observed in the cases of 1.0 and 0.5 μg/ml. In the case of 2.5 μg/ml, the average total number of cell divisions (for a period of 4.5 h) before and after the addition of the drug were 433 ± 112 and 63 ± 7 (s.d. $n = 4$), respectively. The average total number of dividing cells was reduced by ~80%. However, when the concentration was further reduced to 1 and 0.5 μg/ml, the effect was less pronounced. The average total number of cell divisions before the addition of the drug for 1.0 and 0.5 μg/ml were 310 ± 35 and 327 ± 18 (s.d. $n = 4$), respectively. After the addition of the drug, the average total number of dividing cells was reduced by ~50% in both the cases (128 ± 34 and 131 ± 14 for 1 and 0.5 μg/ml, respectively). These results demonstrate a rapid effect of ActD on cell proliferation at 2.5 μg/ml compared to the less intense effect at 1 and 0.5 μg/ml.

example in Fig. 2, the cell divides along the longest axis prior to cell division.

4.3 *Detection of Cell Division in Confluent Cell Cultures*

In cases of highly confluent cell cultures, the pattern corresponding to cell division is not efficiently identified since the pattern, in some cases, is masked by the neighboring cells. However, by using temperature-controlled lensfree video-microscope to acquire images at 4-min intervals, we show that the identification of dividing cells becomes possible in highly confluent cell cultures by detecting cell retraction. Retracting cells exhibit a pattern where the center of the holographic pattern is bright, while the edges are dark (similar to Fig. 2, images at T0 + 0 h 52 min and T0 + 0 h 54 min). By detecting these alternating bright and dark intensity regions in an image, retracting cells were identified (Video 2). However, further criteria are to be added to minimize the false positives and false negatives, which would be a future perspective.

For the work presented here, we could monitor in parallel up to three culture plates (35 mm diameter) with three lensfree video-microscopes having imaging sensor of dimensions 5.7×4.2 mm. The throughput can be dramatically increased by multiplexing 96 smaller sensors to read 96-well plates,[47] which would be an ideal setting for drug screening applications. The method could also be exploited to monitor cell behavior in a bioreactor.

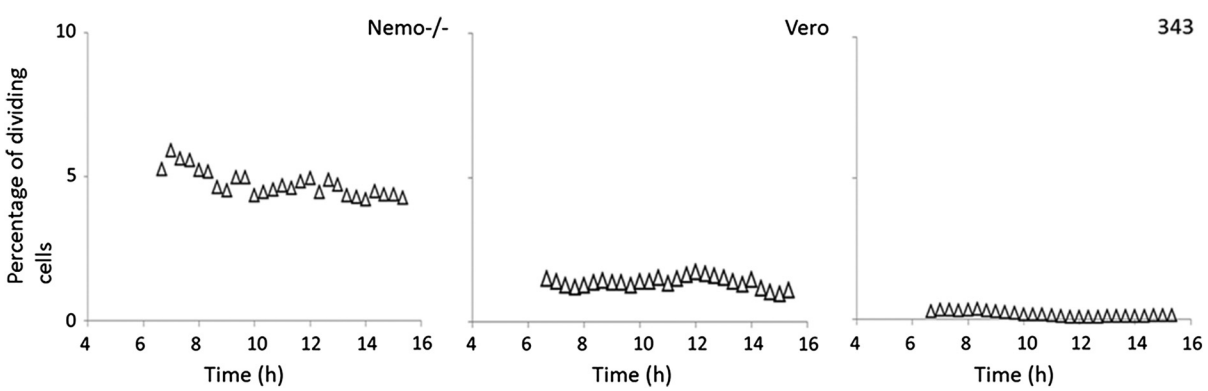

Fig. 8 The kinetics of cell division of three cell types, Nemo$^{-/-}$ (immortalized fetal fibroblasts), Vero (kidney cells from *Cercopithecus aethiops*), and 343 (primary human fibroblasts), followed for a period of 16 h. Moving average (of the percentage of dividing cells) with a period of 2.5 h is depicted in the graph. Note that the percentage of dividing cells in immortalized Nemo$^{-/-}$ cells is higher compared to Vero and primary human fibroblasts (343) cells. In the case of 343 cells, only very few cell divisions (<5) were observed in an image, and hence, the percentage is very low.

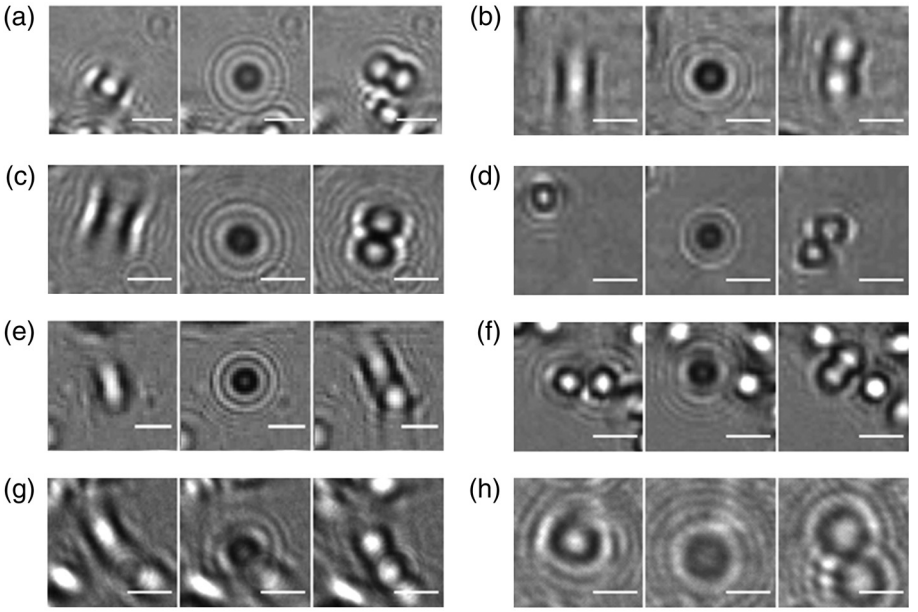

Fig. 9 Other cell types exhibiting similar holographic pattern during cell division: (a) MCF10A, (b) RPE1, (c) U87 cells, (d) RWPE1, (e) mesenchymal stem cells, (f) PC3, (g) HUVEC, (h) RWPE1 in three-dimensional cell culture. Scale bar: 50 μm.

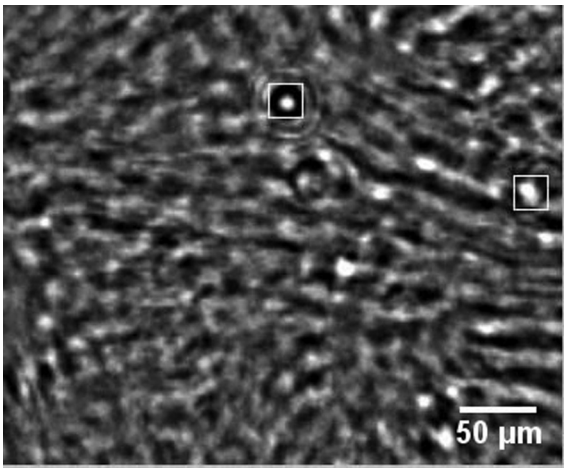

Video 2 Video of highly confluent RPE1 cells showing automated detection of dividing cells. Since the images were acquired at 4-min intervals, cell retraction was clearly observed in dividing cells. Hence cell retraction was detected (Materials and Methods) to detect dividing cells. The detected cells are boxed in white square. This method needs further validation, which would be a future perspective. Frames were acquired every 4 min for ~2 h. Scale bar: 50 μm. (mov, 516 KB) [URL: http://dx.doi.org/10.1117/1.JBO.19.3.036004.2].

5 Conclusion

In sum, we have demonstrated a real-time, label-free, high-throughput, cell proliferation assay that does not involve cell harvesting. The assay is not constrained by the limitations faced by currently used proliferation assays. Lensfree video proliferation assay is direct as it is based on automated detection of single cell divisions over a large FOV, eliminating the use of surrogate measurements. The ability to monitor cell proliferation kinetics profoundly increases the simplicity of studying the time-dependent effects of, e.g., drugs, siRNAs, toxins, etc., on cell proliferation. Since the cell culture remains totally unperturbed, the method is particularly suitable for rare cell types. By demonstrating the possibility of detection of dividing cells in a highly confluent cell culture, we show the applicability of the assay over a very broad range of sample population, from a few hundred to tens of thousands of cells. With increased temporal resolution, we also put forth the possibility of detailed analysis of single cell divisions in a population.

Acknowledgments

The authors wish to thank L. Herve for his help with MATLAB® programming. We wish to thank R. Sauze for the image acquisition software. We thank H. Grateau and T. Bordy for the fabrication of the lensfree video-microscopy setup. We also thank V. Haguet, P. Obeid, D. Freida, E. Sulpice, M. Burute, B. Van der Sanden, M. Dolega, and N. Picollet-D'Hahan for providing us with various cell types. We thank F. Abeille for the help with cell culture experiments.

References

1. H. Gratzner, "Monoclonal antibody to 5-bromo- and 5-iododeoxyuridine : a new reagent for detection of DNA replication placental mononuclear phagocytes as a source of interleukin-1," *Science* **218**(4571), 474–475 (1982).
2. M. P. Siegers et al., "Determination of rates of DNA synthesis in cultured mammalian cell populations," *J. Cell Biol.* **62**(2), 305–315 (1974).
3. A. Salic and T. J. Mitchison, "A chemical method for fast and sensitive detection of DNA synthesis in vivo," *Proc. Natl. Acad. Sci. U. S. A.* **105**(7), 2415–2420 (2008).
4. J. Crouch et al., "The use of ATP bioluminescence as a measure of cell proliferation and cytotoxicit," *J. Immunol. Methods* **160**(1), 81–88 (1993).
5. S. A. Ahmed, R. M. Gogal, and J. E. Walsh, "A new rapid and simple non-radioactive assay to monitor and determine the proliferation of lymphocytes: an alternative to [3H]thymidine incorporation assay," *J. Immunol. Methods* **170**(2), 211–224 (1994).
6. L. J. Jones et al., "Sensitive determination of cell number using the CyQUANT cell proliferation assay," *J. Immunol. Methods* **254**(1–2), 85–98 (2001).

7. M. V. Berridge, P. M. Herst, and A. S. Tan, "Tetrazolium dyes as tools in cell biology: new insights into their cellular reduction," *Biotechnol. Annu. Rev.* **11**(05), 127–152 (2005).
8. S. Al-Nasiry et al., "The use of Alamar Blue assay for quantitative analysis of viability, migration and invasion of choriocarcinoma cells," *Hum. Reprod.* **22**(5), 1304–1309 (2007).
9. I. Giaever and C. R. Keese, "Monitoring fibroblast behavior in tissue culture with an applied electric field," *Proc. Natl. Acad. Sci. U. S. A.* **81**(12), 3761–3764 (1984).
10. C. Xiao et al., "Assessment of cytotoxicity using electric cell-substrate impedance sensing: concentration and time response function approach," *Anal. Chem.* **74**(22), 5748–5753 (2002).
11. P. Upadhyay and S. Bhaskar, "Real time monitoring of lymphocyte proliferation by an impedance method," *J. Immunol. Methods* **244**(1–2), 133–137 (2000).
12. J. Hong et al., "Electrical cell-substrate impedance sensing as a non-invasive tool for cancer cell study," *Analyst* **136**(2), 237–245 (2011).
13. D. R. Tyson et al., "Fractional proliferation: a method to deconvolve cell population dynamics from single-cell data," *Nat. Methods* **9**(9), 923–928 (2012).
14. F. D. Sigoillot et al., "A time-series method for automated measurement of changes in mitotic and interphase duration from time-lapse movies," *PLoS One* **6**(9), e25511 (2011).
15. N. Harder et al., "Automatic analysis of dividing cells in live cell movies to detect mitotic delays and correlate phenotypes in time," *Genome Res.* **19**(11), 2113–2124 (2009).
16. M. Held et al., "CellCognition: time-resolved phenotype annotation in high-throughput live cell imaging," *Nat. Methods* **7**(9), 747–754 (2010).
17. B. Kemper et al., "Label-free quantitative cell division monitoring of endothelial cells by digital holographic microscopy," *J. Biomed. Opt.* **15**(3), 036009 (2010).
18. A. Greenbaum et al., "Imaging without lenses: achievements and remaining challenges of wide-field on-chip microscopy," *Nat. Methods* **9**(9), 889–895 (2012).
19. O. Mudanyali et al., "Wide-field optical detection of nanoparticles using on-chip microscopy and self-assembled nanolenses," *Nat. Photonics* **7**(3), 247–253 (2013).
20. Y. Hennequin et al., "Optical detection and sizing of single nanoparticles using continuous wetting films," *ACS Nano* **7**(9), 7601–7609 (2013).
21. S. A. Lee et al., "On-chip continuous monitoring of motile microorganisms on an ePetri platform," *Lab Chip* **12**(13), 2385–2390 (2012).
22. G. Jin et al., "Lens-free shadow image based high-throughput continuous cell monitoring technique," *Biosens. Bioelectron.* **38**(1), 126–131 (2012).
23. M. E. Dolega et al., "Label-free analysis of prostate acini-like 3D structures by lensfree imaging," *Biosens. Bioelectron.* **49C**, 176–183 (2013).
24. M. Théry and M. Bornens, "Cell shape and cell division," *Curr. Opin. Cell Biol.* **18**(6), 648–657 (2006).
25. K. Suzuki and K. Takahashi, "Reduced cell adhesion during mitosis by threonine phosphorylation of beta1 integrin," *J. Cell. Physiol.* **197**(2), 297–305 (2003).
26. E. Boucrot and T. Kirchhausen, "Mammalian cells change volume during mitosis," *PLoS One* **3**(1), e1477 (2008).
27. S. Stenman, J. Wartiovaara, and A. Vaheri, "Changes in the distribution of a major fibroblast protein, fibronectin, during mitosis and interphase," *J. Cell Biol.* **74**(2), 453–467 (1977).
28. J. Baker and D. Garrod, "Epithelial cells retain junctions during mitosis," *J. Cell Sci.* **104**(2), 415–425 (1993).
29. A. G. Clark and E. Paluch, "Mechanics and regulation of cell shape during the cell cycle," in *Cell Cycle in Development*, J. Z. Kubiak, Ed., pp. 31–73, Springer, Berlin, Heidelberg (2011).
30. M. Théry and M. Bornens, "Get round and stiff for mitosis," *HFSP J.* **2**(2), 65–71 (2008).
31. M. P. Stewart et al., "Hydrostatic pressure and the actomyosin cortex drive mitotic cell rounding," *Nature* **469**(7329), 226–230 (2011).
32. L. P. Cramer and T. J. Mitchison, "Investigation of the mechanism of retraction of the cell margin and rearward flow of nodules during mitotic cell rounding," *Mol. Biol. Cell* **8**(1), 109–119 (1997).
33. P. Kunda et al., "Moesin controls cortical rigidity, cell rounding, and spindle morphogenesis during mitosis," *Curr. Biol.* **18**(2), 91–101 (2008).
34. A. S. Maddox and K. Burridge, "RhoA is required for cortical retraction and rigidity during mitotic cell rounding," *J. Cell Biol.* **160**(2), 255–265 (2003).
35. Y.-W. Heng and C.-G. Koh, "Actin cytoskeleton dynamics and the cell division cycle," *Int. J. Biochem. Cell Biol.* **42**(10), 1622–1633 (2010).
36. O. M. Lancaster et al., "Mitotic rounding alters cell geometry to ensure efficient bipolar spindle formation," *Dev. Cell* **25**(3), 270–283 (2013).
37. A. W. Murray, "Creative blocks: cell-cycle checkpoints and feedback controls," *Nature* **359**(6396), 599–604 (1992).
38. M. J. O'Connell, C. Nancy, and A. M. Carr, "The G2-phase DNA-damage checkpoint," *Trends Cell Biol.* **10**(07), 296–303 (2000).
39. J. Melo and D. Toczyski, "A unified view of the DNA-damage checkpoint," *Curr. Opin. Cell Biol.* **14**(2), 237–245 (2002).
40. U. Hollstein, "Actinomycin. Chemistry and mechanism of action," *Chem. Rev.* **74**(6), 625–652 (1973).
41. H. M. Sobell, "Actinomycin and DNA transcription," *Proc. Natl. Acad. Sci. U. S. A.* **82**(16), 5328–5331 (1985).
42. N. Minc, D. Burgess, and F. Chang, "Influence of cell geometry on division-plane positioning," *Cell* **144**(3), 414–426 (2011).
43. M. Théry et al., "The extracellular matrix guides the orientation of the cell division axis," *Nat. Cell Biol.* **7**(10), 947–953 (2005).
44. T. E. Gillies and C. Cabernard, "Cell division orientation in animals," *Curr. Biol.* **21**(15), R599–609 (2011).
45. C. Panbianco and M. Gotta, "Coordinating cell polarity with cell division in space and time," *Trends Cell Biol.* **21**(11), 672–680 (2011).
46. D. Odde, "Getting cells and tissues into shape," *Cell* **144**(3), 325–326 (2011).
47. V. Haguet et al., "Parallelized lensfree time-lapse microscopy," in *Conf. NanoBioEurope, 10-12 June 2013*, Toulouse, France, NanoBioEurope (2013).

Biographies of the authors not available.